SSCL-340

Superconducting Super Collider Laboratory

SSCL-340

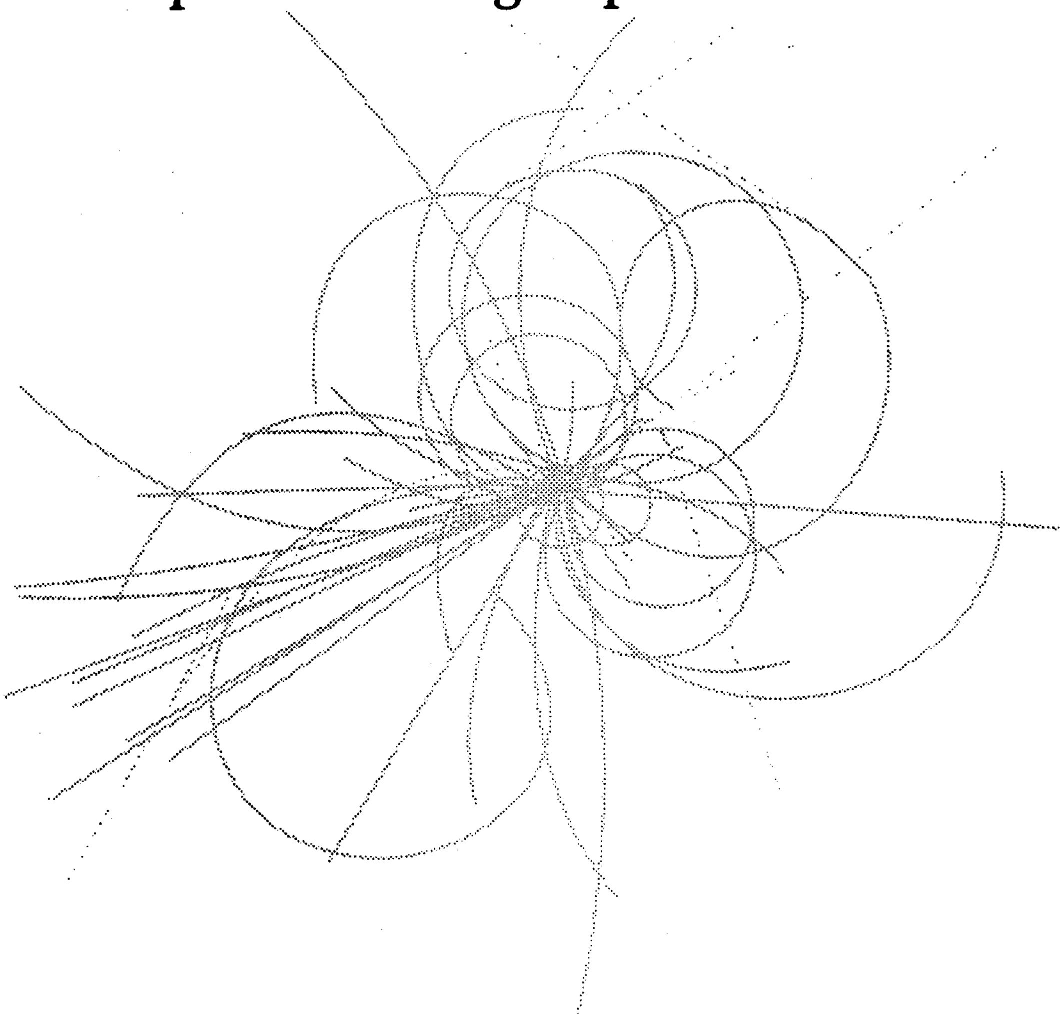

Phase-Control Scheme for Synchronous Beam Transfer from the Low Energy Booster to the Medium Energy Booster

L. K. Mestha

September 1991

SSCL-340

Phase-Control Scheme for Synchronous Beam Transfer from the Low Energy Booster to the Medium Energy Booster

L. K. Mestha

Accelerator Systems Division
Superconducting Super Collider Laboratory*
2550 Beckleymeade Avenue
Dallas, TX 75237

September 1991

* Operated by the Universities Research Association, Inc., for the U.S. Department of Energy under Contract No. DE-AC35-89ER40486.

SSCL-340

Phase-Control Scheme for Synchronous Beam Transfer from the Low Energy Booster to the Medium Energy Booster

L. K. Mestha

Abstract

This report discusses the design philosophy of the new synchronization scheme for beam transfer from the Low Energy Booster (LEB) to the Medium Energy Booster at the Superconducting Super Collider. The fundamental principle of controlling the LEB acceleration is discussed. A generalized mathematical model is derived to facilitate the design of multiple feedback loops to control the synchronizing phase and the radial position of the beam. Applications of state feedback, sliding-mode and model reference controllers are discussed. Although the state feedback controller is easy to design and implement, the simulation results show that the controller properties are not useful to handle disturbance due to field errors and variation in the system parameters. The sliding-mode and model reference controllers are shown to have more suitable properties. At the end, mention of the hardware used to establish the "proof of principle" is given.

1.0 INTRODUCTION

For extraction purpose, the phase of the Low Energy Booster (LEB) must be adjusted to match the phase of the Medium Energy Booster (MEB) rf. The SCDR LEB rf sweeps from 47.5 MHz to 59.776 MHz in 50 milliseconds. During transfer the MEB rf is designed to run exactly at the LEB extraction frequency. In the literature one sees two schemes[1,2] for achieving synchronous transfer of bunched beams: the phase-locking and the phase-slippage schemes. In the phase-locking scheme, at a known time before injection to the next accelerator, the phase and frequency of the accelerating machine are locked to the extraction frequency. The time required to phase lock the two frequencies depends on the lattice parameters of the accelerating machine.[3] In the phase-slippage scheme, at a predetermined time before transfer, the frequency of the accelerating machine is offset a few cycles relative to the extraction frequency. As a result, the phase of the accelerating frequency slips relative to the fixed frequency, and several phase coincidence points of the reference wave occur at a beat frequency equal to the offset frequency. One of them is used to trigger the synchronous transfer of the beam.

A more general approach for synchronization is to consider the "locking" of the phase of the variable frequency source with the phase of the fixed frequency source throughout the acceleration. Since the fundamental concept of this approach consists of maintaining control of the phase with a suitable feedback mechanism, it is more appropriate to call it the "phase-control" scheme. In this scheme the rf wave (also called the reference rf wave) is forced to follow a pre-programmed "trip-plan" so that at the instant of transfer it will have the same phase as the MEB rf wave (except for constant phase offset). A feedback loop corrects for any deviation from the trip-plan. The trip-plan has at least one point at flat B-field region where the machines have exact phase for the purpose of synchronous beam transfer. With this scheme it is possible to synchronize two rf sources starting from a random phase difference. Since the approach consists of maintaining the longitudinal phase relationship to a known trajectory, the control of the transverse position is also necessary. We have emphasized here the need of a global feedback which not only provides the right accelerating frequency by keeping control of the transverse position, but also maintains a definite phase relationship with the next accelerator. By following this approach we would need to spend less time for cogging during extraction. With the existing schemes, the synchronization loops come into effect just before the extraction.

We have analyzed an isolated case by considering the feedback loop for the longitudinal phase synchronization only. The discussion of the transverse feedback, when included with the synchronization loop, becomes more involved and is not shown here. The feedback loop is analyzed with three different types of modern feedback controllers for the single-input single-output case (input as the rf frequency shift and the output as the phase difference between the designated rf waves of the two machines). A few comparisons are made using the simulated results.

2.0 TRIP-PLAN

As mentioned earlier, the trip-plan is the pre-programmed trajectory calculated from the two reference rf waves, one from each machine. Since this is the ideal trajectory, the actual trajectory changes in the presence of field errors. We can calculate the time at which the two reference rf waves match under ideal circumstances as follows. The phase of the LEB reference rf wave from a given time during acceleration is equal to

$$\Psi_{\mathrm{LEB}} = \frac{2\pi}{h} \int_0^{\tau} Rf(t)dt. \tag{1}$$

Similarly the phase of the MEB reference rf wave can be written as

$$\Psi_{\mathrm{MEB}} = \frac{2\pi R'}{h'} f'\tau. \tag{2}$$

The notations R and R' are the radii of the orbits, f and f' are the rf frequencies, and h and h' are the harmonic numbers of the LEB and the MEB, respectively;

τ is the time interval over which the integration is carried out. The difference between Equations 2 and 1 is the "synchronizing phase," Ψ. That is,

$$\Psi = |\Psi_{\mathrm{MEB}} - \Psi_{\mathrm{LEB}}|. \tag{3}$$

For synchronous transfer, the synchronizing phase is equal to zero (ignoring the transfer line delays). Because the present discussion is for two circular machines with non-integer circumference ratios (22/3), the LEB reference rf wave will have completed several full turns and a semi-turn at the end of one MEB turn. If the two frequencies are the same, then the LEB reference rf wave completes 7 full turns and a semi-turn equal to one-third the LEB circumference, which is the case with flat B-field. The semi-turn is not one-third the circumference ratio when the frequencies are different. Equation 3 is plotted in Figure 1 for each MEB turn. The "+" marks represent the position of the LEB reference rf wave for each MEB turn away from the transfer point. The phase values are shown from 0 to 540 meters to cover the full circumference of the LEB. Path length representing full turns completed by the LEB reference wave is ignored, since it is of no significance for synchronization. Figure 1 shows three curves approaching constancy at 50 msec; this is due to the fraction "1/3" in the circumference ratio. The decay results from the narrowing of difference in frequencies as the transfer time approaches when the magnetic field is at its maximum. In this region every third point is on the same curve. This means the relative phasing between the two reference waves is constant every time the MEB reference wave completes three turns.

The synchronizing phase as seen in Figure 1 is not zero for transfer purposes. Also, if the LEB reference wave is controlled to the trip-plan shown in Figure 1, there may be synchronization with the MEB reference wave, but transfer cannot be matched. Instead, if the trip-plan is offset by 111.78 meters right at the beginning and an arbitrary rf wave is arranged to follow the new synchronizing phase, then there will be several transfer points. The new trip-plan is shown in

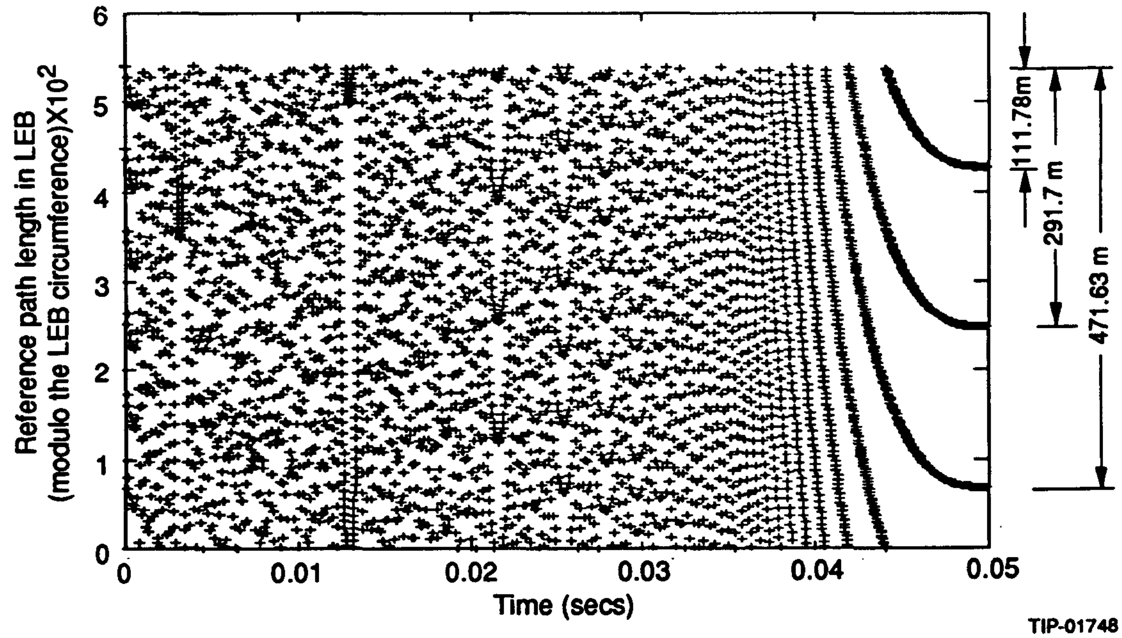

Figure 1. Synchronizing Phase During Acceleration in the LEB. Phase not adjusted.

Figure 2, where the turn numbers, such as 3771 and 3774, have zero phase. We must remember at this stage that the trip-plan shown in Figures 1 and 2 were computed by changing the frequency at all times from injection to extraction. However, in an actual system, the acceleration takes place only at the rf cavity positions. Figure 3 shows the trip-plan when there is only one cavity in the SCDR lattice.

3.0 SYSTEM MODEL

3.1 Equation for Synchronizing Phase Error

The synchronizing phase is a function of the beam orbit and the accelerating frequency. The errors in the beam orbit and frequency introduce errors in the synchronizing phase. The system model can be obtained by introducing error terms in the beam orbit and the frequency in Equation (1). Let $\Delta R(t)$ be the

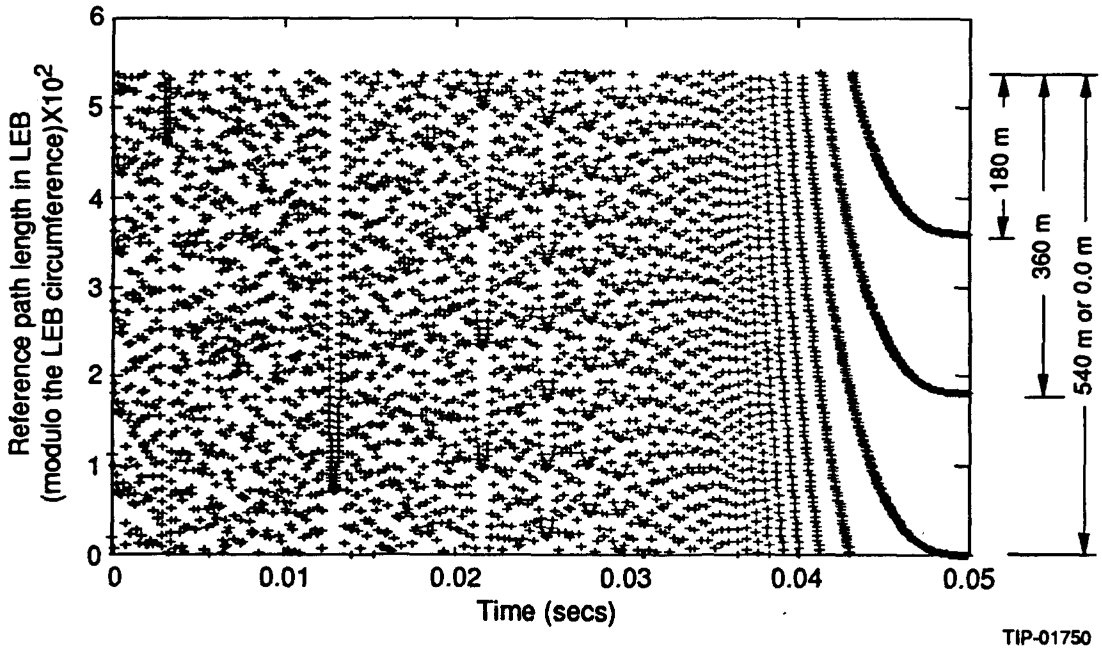

Figure 2. LEB Trip-Plan. Phase adjusted to zero at transfer time.

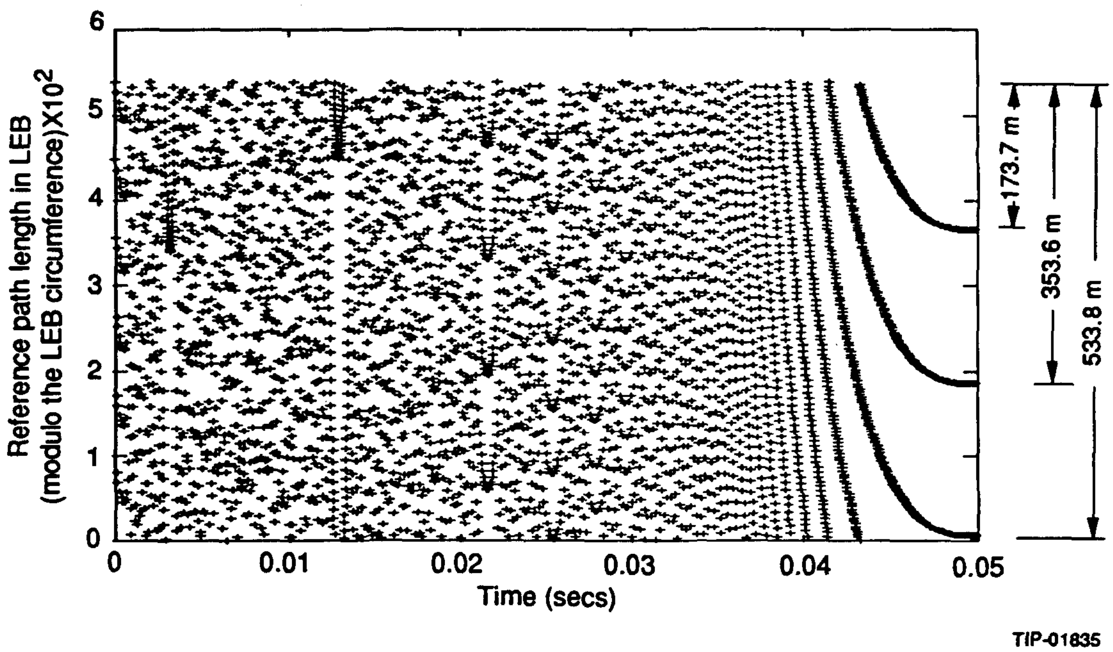

Figure 3. LEB Trip-Plan. With one RF cavity and phase not adjusted.

total deviation in the radius of the orbit and $\Delta f(t)$ be the error in the master frequency; then the phase equation becomes

$$\Psi'(t) = \frac{2\pi}{h} \int [R + \Delta R(t)]\,[f(t) + \Delta f(t)]\,dt. \tag{4}$$

The sign of $\Delta R(t)$ depends on which side of transition the machine is operating. Because the control philosophy is to maintain the trip-plan discussed earlier by modulating the LEB frequency, an equation for the error in synchronizing phase in terms of the frequency is required. This phase error is equal to the offset in the path length covered by the LEB reference wave from the ideal path. Hence it is given by

$$\delta\Psi(t) = \Psi'(t) - \Psi_{\mathrm{LEB}}(t) \tag{5}$$

Substituting Equations 1 and 4 in Equation 5 and taking the first derivative with respect to time, the following differential equation is obtained:

$$\frac{d[\delta\Psi(t)]}{dt} = \frac{2\pi}{h}\left[\Delta R(t) f(t) + R\Delta f(t) + \Delta R(t)\Delta f(t)\right]. \tag{6}$$

For small changes in the orbit shift and the frequency, $\Delta R(t)$ and $\Delta f(t)$ can be replaced by $\delta R(t)$ and $\delta f(t)$. Hence the product of $\delta R(t)$ and $\delta f(t)$ becomes negligible. However, at this stage we can retain the second order terms. Furthermore, the error in the radial orbit shift can be obtained as described in the following section.

3.2 Equation for Radial Orbit Shift

The error in the average shift in the beam orbit from the ideal orbit can be obtained from the momentum equation

$$p(t) = eB(t)\rho(t), \tag{7}$$

where e is the charge in Coulombs, B the bending field in Tesla, and ρ is the effective bending radius of the particle in meters. When there is error in the bending field, $\delta B(t)$, the effective bending radius of the off-momentum particle changes. Hence by using the partial fraction expansion,

$$\delta p(t) = \frac{\partial p}{\partial B}\delta B(t) + \frac{\partial p}{\partial \rho}\delta \rho(t), \tag{8}$$

and dividing Equation 8 by Equation 7 and simplifying, we obtain

$$\frac{\delta p(t)}{p(t)} = \frac{\delta B(t)}{B(t)} + \left[\frac{1}{p(t)}\frac{\partial p}{\partial \rho}\delta \rho(t)\right]. \tag{9}$$

The terms within the brackets can be argued to equal:

$$\frac{1}{p(t)}\frac{\partial p}{\partial \rho}\delta \rho(t) = \gamma_T^2 \frac{\delta R(t)}{R}. \tag{10}$$

The momentum variation $\delta p(t)/p$ can also be expressed in terms of the orbit shift $\delta R(t)$ and the frequency shift $\delta f(t)$, as follows:

$$\frac{\delta p(t)}{p(t)} = \gamma^2(t)\left[\frac{\delta R(t)}{R} + \frac{\delta f(t)}{f(t)}\right]. \tag{11}$$

From Equations 9, 10, and 11, $\delta R(t)$ is written as follows:

$$\delta R(t) = \left[\frac{\gamma^2(t) R}{\gamma_T^2 - \gamma^2(t)}\right]\left[\frac{\delta f(t)}{f(t)} - \frac{1}{\gamma^2(t)}\frac{\delta B(t)}{B(t)}\right]. \tag{12}$$

This equation shows that the orbit shift $\delta R(t)$ can be minimized by shifting the frequency due to the field errors. Although a feedback loop to the magnet system would minimize the orbit shift, it is impractical to embark on this approach due to a long time constant of the magnet system. Thus, to minimize $\delta\Psi(t)$ and $\delta R(t)$ in the presence of field errors, we would have to change $\delta f(t)$. From the point of view of feedback control, this amounts to a one-input [$\delta f(t)$] and two-output [$\delta\Psi(t)$ and $\delta R(t)$] system. To add more flexibility to the feedback system, we can include an additional input: the phase of the center of the beam bunch with respect to the zero cross over of the rf wave. That is, by shifting the rf relative to the beam by an amount $\delta\phi(t)$ we can minimize the radial orbit shift. System equation to accommodate this input is shown below.

3.3 Equation for RF Phase Shift

If $\phi(t)$ is the phase of the center of the beam bunch with respect to the zero cross-over of the rf signal, $\delta f(t)$ is the additional phase shift imposed by moving the rf signal, and $V(t)$ is the amplitude of the cavity voltage, then the energy gain per turn (assuming one rf cavity) is given by

$$\Delta E(t)|_{\mathbf{turn}} = eV(t)\sin\phi(t). \tag{13}$$

For a small increment in energy per turn, $\Delta E(t)$ can be approximated to $\delta E(t)$ and hence can be replaced by the product of the incremental momentum change and the linear velocity, $v(t)$. Thus Equation 13 is written as

$$v(t)\,\delta p(t)|_{\mathbf{turn}} = eV(t)\sin\phi(t), \tag{14}$$

or, more appropriately,

$$\frac{\delta p(t)}{\delta t} = \frac{eV(t)}{2\pi R}\sin\phi(t). \tag{15}$$

From Equation 8, the derivative of the momentum with respect to time can be written as follows:

$$\frac{\delta p(t)}{\delta t} = \frac{\partial p}{\partial B}\frac{\delta B(t)}{\delta t} + \frac{\partial p}{\partial \rho}\frac{\delta \rho(t)}{\delta t}. \tag{16}$$

The time derivative of $\rho(t)$ is assumed to be small for our control purpose. After approximation, Equation 7 is substituted in Equation 16, with the result compared to Equation 15. Hence we determine that

$$V(t)\sin\phi(t) = 2\pi R\rho\,\frac{dB(t)}{dt}. \tag{17}$$

By taking the partial derivative of the left hand side with respect to $V(t)$ and $\phi(t)$, and the partial derivative of the right hand side with respect to R, ρ and

dB/dt, and ignoring the incremental change in $\delta\rho$, the following relationship for $\delta\phi(t)$ is obtained:

$$\delta\phi(t) = \frac{2\pi R\rho}{V(t)\cos\phi(t)}\frac{d[\delta B(t)]}{dt} - \tan\phi(t)\left[\frac{\delta V(t)}{V(t)} - \frac{\delta R(t)}{R}\right]. \tag{18}$$

Although the variables $\delta B(t)$ and $\delta V(t)$ can be measured, we can regard them as disturbances to the system.

4.0 FEEDBACK CONTROLLER

Equations 6, 12, and 18 constitute the system model. The system for the LEB is linear and time-varying. Our purpose at this stage is to minimize the error in synchronizing phase, while not perturbing the radial position to uncontrollable values. Using the system equations, we calculate the controller to generate the shift in phase and frequency. A simplified block diagram of a possible system is shown in Figure 4. The coefficients of the system equations are calculated with respect to time for the ideal case. The input to the controller consists of ideal parameters such as the accelerating frequency, phase of the center of the bunch with respect to rf wave, cavity voltage profile, and magnetic field profile. The deviations of the cavity voltage and the magnetic field can be obtained by measuring their actual value and comparing them with their respective ideal values. They can be treated as disturbances to the controller.

There are several types of controllers one can design to make the loop stable. For a linear time-invariant system and a single-input single-output feedback loop, there are number of frequency domain techniques available. Well-established controllers include the Proportional Integral, Proportional Integral Derivative, Phase-Lag, and Phase-Lead types. For a linear, time-invariant multi-input multi-output system, the inverse Nyquist array or decoupling method are widely used. Although these techniques can be applied by narrowing the problem to a small time-invariant region, the controller will not be adaptive and has no robustness to parameter variation and external disturbance. In this context the term "adaptive" means the ability of the controller to adjust to changes in the parameters

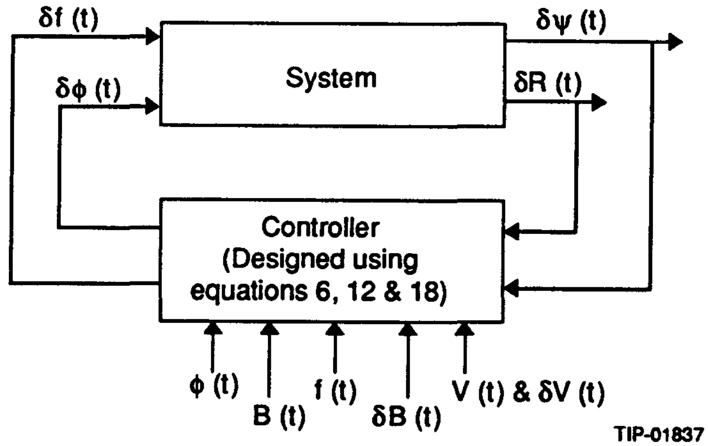

Figure 4. Schematic Block Diagram of the Two-Input Two-Output Feedback Loop.

such that the synchronizing phase and the radial beam position converge to a desired value. In other words the controller would be able to track the variation in the parameters. Some of the time-domain techniques based on linear state feedback theory cannot be applied to our problem since they are very sensitive to parameter variations. The nature of the system requires a more sophisticated and mathematically sound feedback controller. Controllers based on two different techniques may meet the requirement. One of them is known as Model Reference Adaptive Controller (MRAC), and the other as Sliding-Mode controller (SMC).

In the MRAC, a reference model is chosen, the structure and parameters of which are well-defined to suit the desired radial position and synchronizing phase. The reference model output is compared with the system output. Error is then processed in the controller such that the output of the controller driving the system is able to produce the desired beam radius and phase. Sometimes, the presence of unmodelled process dynamics may induce instability in the control loop, leading to beam loss and loss of synchronization. An alternative could be to use an adaptive adjustment of the reference model or a sliding-mode controller.

In the sliding-mode controller, adaptive mechanisms are built into the feedback loop once the limits on the parameters are known.

To understand the principle of advanced feedback controllers, we have simplified the problem by not considering the radial position feedback loop. With this condition, the input end in Figure 4 will have no variation imposed by the controller to the rf phase. The feedback system will therefore simplify to single-input $[\delta f(t)]$ single-output $[\delta\Psi(t)]$ type. We have made an attempt here to acquaint the reader with the design of three controllers for the simple single-input, single-output case. The present report therefore contains the design philosophy of the simplified loop. The more complicated multiple-loop situation is not discussed here. The system equation for a single-input single-output case is obtained by using Equation 12 in Equation 6 above. The non-linear terms are retained, although they contribute very little to the phase error, $\delta\Psi(t)$. After simplification, the following equation is obtained:

$$\begin{aligned}\frac{d\delta\Psi(t)}{dt} = \frac{2\pi R}{h}\left(\frac{\gamma_T^2}{\gamma_T^2-\gamma^2}\right)\delta f(t) + \frac{2\pi R}{hf}\left(\frac{\gamma^2}{\gamma_T^2-\gamma^2}\right)\delta f^2(t) \\ - \frac{2\pi R}{hB}\left(\frac{f}{\gamma_T^2-\gamma^2}\right)\delta B(t) - \frac{2\pi R}{hB}\left(\frac{1}{\gamma_T^2-\gamma^2}\right)\delta B(t)\delta f(t)\end{aligned} \tag{19}$$

The system represented by Equation 19 has terms related to variation in the bending field. For the purpose of designing the controller we can ignore the field perturbations, i.e., $\delta B(t) = 0$, and design the feedback loop, which generates the right amount of frequency shift such that $\delta\Psi(t)$ is minimized to zero. Once the controller is designed, we will simulate the loop performance by using Equation 20 above as system with the effect of field variation included. We will also analyze the robustness of the feedback loop with disturbance at the input end.

It will be convenient if we use Equation 19 in a general state-space form[4,5] with A, B and C as system matrices, $u(t)$ the control signal, $y(t)$ the output signal, and $x(t)$ the state variable.

$$\begin{aligned} \dot{x}(t) &= A(t)x(t) + b(t)u(t) \\ y(t) &= C(t)x(t) \end{aligned} \tag{20}$$

Comparing Equation 20 with Equation 19, for $\delta B(t) = 0$, we obtain:

$$\begin{aligned} x(t) &= \delta\Psi(t) \\ A(t) &= 0 \\ b(t) &= \frac{\gamma_T^2}{\gamma_T^2 - \gamma^2} R \\ C(t) &= 1 \\ u(t) &= \delta\omega(t) + \frac{1}{\omega(t)} \left[\frac{\gamma(t)}{\gamma_T}\right]^2 \delta\omega^2(t) \\ \delta\omega(t) &= \frac{2\pi}{h} \delta f(t) \\ \omega(t) &= \frac{2\pi f(t)}{h} \end{aligned} \tag{21}$$

Although the system coefficients $A(t)$, $b(t)$, and $C(t)$ are shown to be time-varying, only the coefficient $b(t)$ has such property. Also note that Equation 19 is now in the linear form which is obtained by grouping coefficients of $\delta f(t)$ and $\delta f(t)^2$ into the control signal $u(t)$. In this particular case, since the control signal is a quadratic in $\delta f(t)$, it turns out that separating $\delta f(t)$ will not be a problem once $u(t)$ is known. Figure 5 shows the schematic system block diagram of Equation 20. The feedback connection will generate the desired control signal $u(t)$. Without the feedback loop, the system model (Equations 20 and 21) shows that the phase error grows as a function of the error in the accelerating frequency. In view of the importance of the control problem, three types of feedback controllers were investigated. The design procedure is quite involved and may appear complicated. On the other hand, the need for such techniques exists in the accelerator environment and must be fully explored.

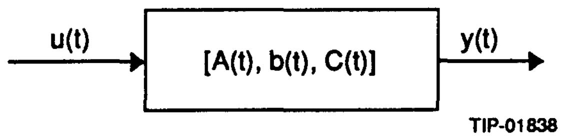

Figure 5. Schematic Block Diagram of the System Represented by Equation 21 Without the Feedback.

5.0 LINEAR STATE-VARIABLE FEEDBACK CONTROLLER

5.1 Determining Feedback Gain

In feedback control jargon, $x(t)$ is called the state of the system. Since we are using the state variable to relocate the eigenvalue of the open loop system to achieve better response characteristics, it is called the State-Variable feedback. This is in fact the modern method of designing the proportional feedback. We will determine the feedback gain by assuming $b(t)$, the system parameter, to be time-invariant. Since $b(t)$ is varying adiabatically (see Figure 6), such an assumption would not introduce errors. With this assumption, we see that the open loop system has a characteristic equation with a single pole at the origin. With the negative feedback gain k as shown in Figure 7, the new state equation of the closed loop system becomes

$$\dot{x}(t) = -bkx(t). \tag{22}$$

Hence, the characteristic polynomial is equal to

$$a_c(s) = s + bk, \tag{23}$$

where s is the Laplace parameter. Since our system is first-order we will have one eigenvalue to select on the left half of the s-plane[5] to obtain a stable closed loop response. The characteristic polynomial of the system with the new eigenvalue, say α_1, is given by

$$\alpha(s) = s + \alpha_1. \tag{24}$$

In order to achieve the new system response as dictated by the eigenvalue α_1, we must have Equation 24 made equal to Equation 23. By comparing, we obtain the feedback gain k. Thus,

$$k = \frac{\alpha_1}{b}. \tag{25}$$

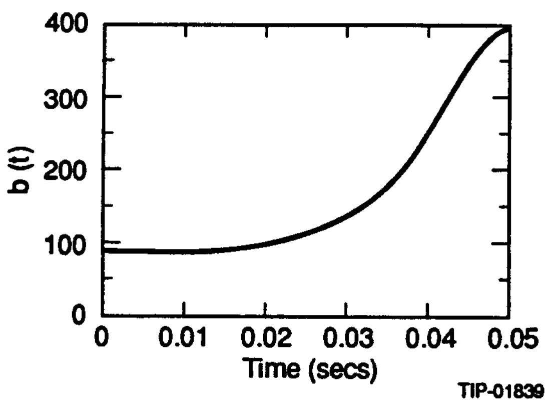

Figure 6. Variation of Function $b(t)$ with Respect to Time.

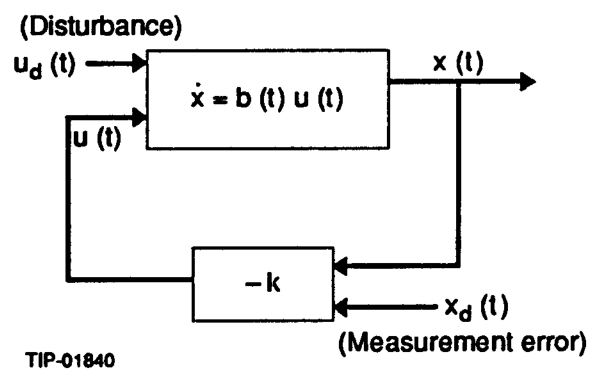

Figure 7. Schematic Block Diagram of the State Variable Feedback Loop.

5.2 Analysis of the Loop Performance

It will be easy to understand the stability of the loop by looking at the phase plane portrait of the system with and without feedback. Figure 8 is a plot of $\dot{x}$ against x for the system Equation 20 for the SCDR LEB with a frequency shift of 1 KHz step. The phase trajectories in the upper half of Figure 8 move right and those on the lower half move left. They grow with the frequency shift, and the trajectories show no signs of meeting at the origin. This means that the time response of the open loop system is divergent. Figure 9 shows the plot of the phase trajectories for the new system represented by Equation 22, with $k = 1$ and 5. Here we see that the system is asymptotically stable whatever the initial conditions on x are, since the trajectories are directed to the origin. The time response for Figure 7 is shown in Figure 10 for $k = 2$ and $k = 20$. Also, Figure 11 shows the corresponding plot of the frequency shift imposed by the feedback loop with respect to time. The state feedback loop will work very well

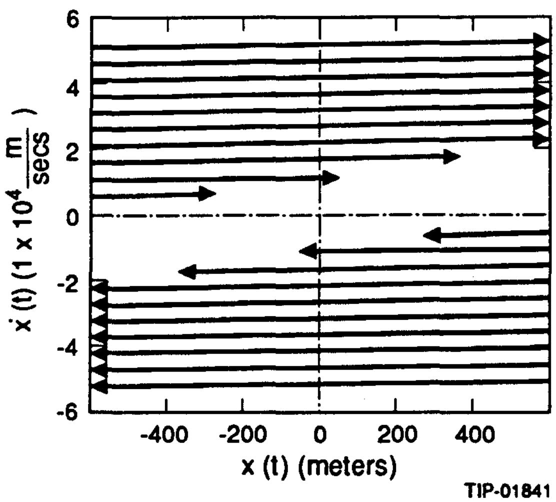

Figure 8. Phase Trajectories for the Open Loop System Equation ($\delta f = 1$ KHz step).

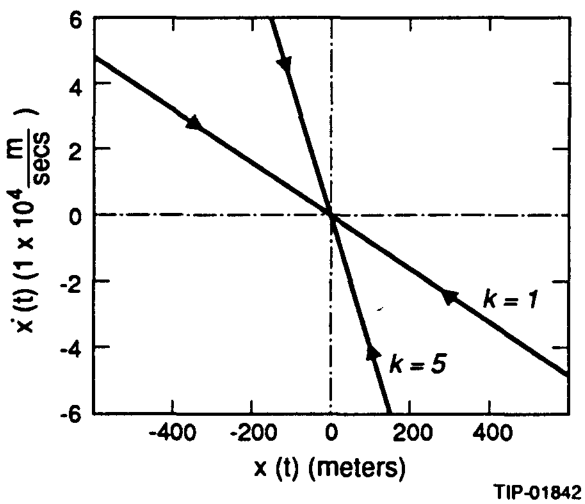

Figure 9. Phase Trajectories for the Closed Loop System Equation.

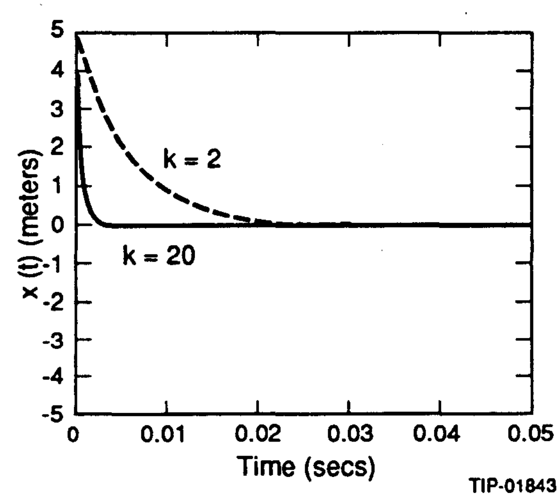

Figure 10. Time Response of the State $x(t)$ with the Feedback Loop Closed.

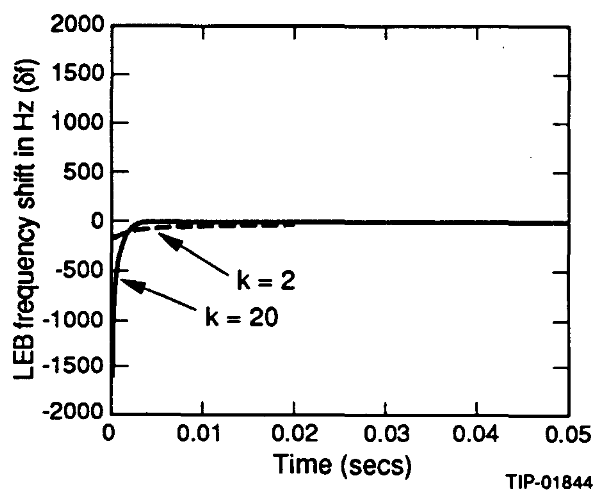

Figure 11. Decay of the Frequency Shift with Respect to Time.

when there is no disturbance on the system. Disturbance could be due to field error or measurement errors in the synchronizing phase. With the field error there is frequency shift, say δf_d, disturbance is represented by u_d in Figure 12. A measure of the amount of disturbance can be obtained from Equation 12 for no orbit shift (i.e., $\delta R = 0$). By substituting Equation 26 in Equation 21, u_d is obtained. In Figure 12 we show the plot of the function u_d for $\delta B/B$ of 5×10^{-4}. Since we worry about the robustness of the loop for about 8 ms

$$\delta f_d = \frac{f(t)}{\gamma^2(t)} \frac{\delta B}{B} \tag{26}$$

before the extraction, we can put a step of magnitude $u_d = 11$ radians, hold it until the extraction time, and observe the time response of the state variable x. This is shown in Figure 13. It is clear that the system is not robust since the phase error is not held zero (or at least to a tolerable value) under external disturbances to the loop. When there is measurement error in the synchronizing phase (i.e., when x_d is not equal to zero in Figure 7), the loop does not show desirable performance. Increasing the feedback gain would reduce the effect, but would invariably enlarge the control signal which leads to increased frequency shift. This will create beam oscillations.

Another useful test is to study the sensitivity of the loop to variation of the system parameters within the operating limits. In our problem, the system parameter is $b(t)$ (see Equation 20) which is a function of the accelerating frequency. To estimate the effect of parameter variation on the phase error, we assumed a change of up to 1% in $b(t)$ in the system equation, and then closed the feedback loop. The loop response was not very different from the ideal curve of Figure 10.

The simulation was also carried out with the system as Equation 19 instead of the simplified system Equation 20. $\delta B(t)$ was assumed to have Gaussian noise with a normal distribution such that

$$\delta B(t) = 5 \times 10^{-4} \, B_{\max} \, [\text{rand(normal)}]. \tag{27}$$

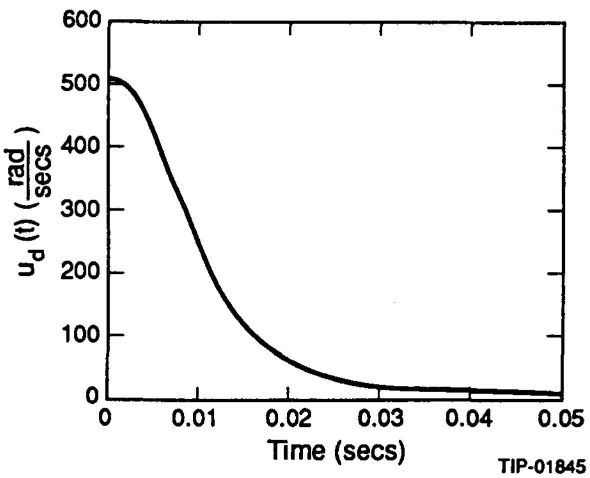

Figure 12. Magnitude of the Expected Disturbance Function u_d for $\delta B/B = 5 \times 10^{-4}$.

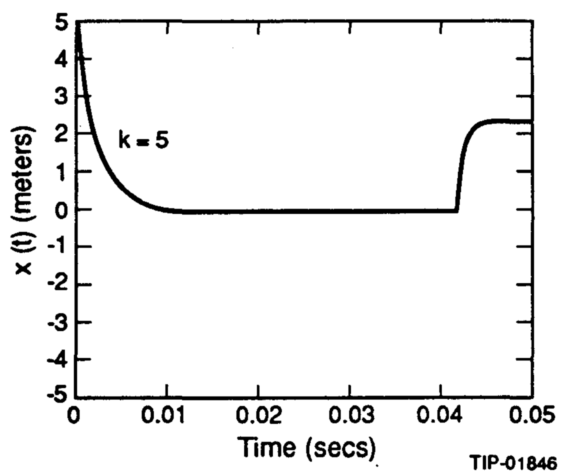

Figure 13. Time Response of the State (Observe the State Changing with a Step Input in Disturbance at 42 ms).

The time response of the phase error plot is shown in Figure 14. Although the above figure shows a controlled minimization of the phase error, we have seen that the state feedback loop is not robust to external disturbance. Alternatively, one may argue to increase the gain of the feedback loop. As we saw earlier this may lead to beam oscillations due to large frequency shift. This suggests that from a practical standpoint the synchronization will not be accurate. Hence an adaptive and a robust controller may look more promising than the state feedback. We discuss at first the design of a sliding-mode controller followed by the model reference adaptive controller.

6.0 SLIDING-MODE CONTROLLER

6.1 Variable Structure System

In the discussion related to linear state feedback, we had considered a negative feedback loop. The structure of the negative feedback is not the same as that of the system with positive feedback. If we now devise a mechanism to switch the negative feedback to positive feedback, we would end up with the phase

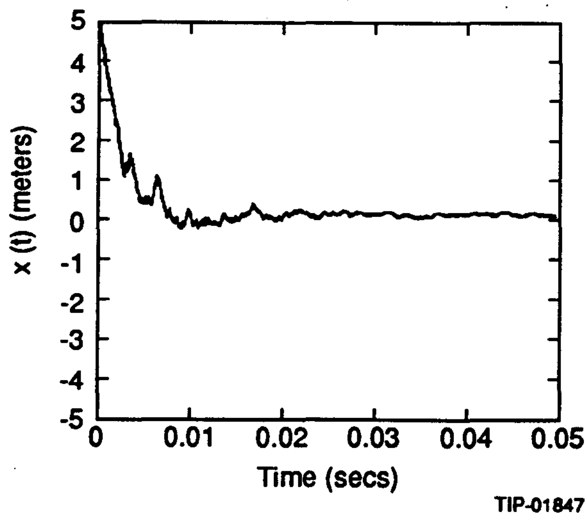

Figure 14. Time Response of the State when the Field Error of 5×10^{-4} is Considered in the System Equation 19.

portraits in the I and III quadrants as shown in Figure 15. However, at this stage the point to emphasize is that by changing the sign of the feedback loop, we basically toggle the structure of the system from one state to another. Such a feedback control system, where the structure of the system is altered, is known as a Variable Structure System (VSS). The sliding-mode control is a subset of the Variable Structure System. Here we intentionally switch the sign of the feedback whenever a selected point in the x-$\dot{x}$ coordinates, called the representative point, crosses certain boundaries. The theory behind the sliding-mode control is quite involved. The reader is urged strongly to refer to the only known book in the literature, by U. Itkis,[6] for a detailed explanation of the basic principles of the subject. This book deals with a more classical sliding-mode controller design. More up-to-date information can be obtained from the research papers, and some of them are listed in this report.[7–9] The modern sliding-mode controller has been heavily modified to include additional features.

The basic design of the sliding-mode control system is divided into the methods of selection of the switching line and appropriate substructures of the feedback

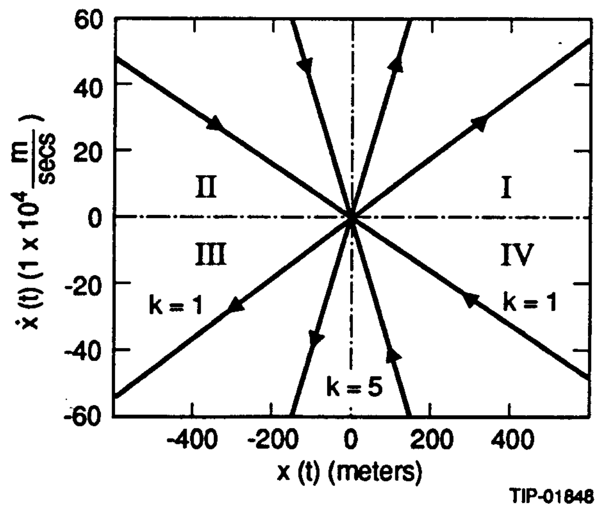

Figure 15. Phase Trajectories.

controller. In our problem we consider the switching line in the IV quadrant of Figure 15, such that the slope of the line α is under our control. Thus the following equation can be considered as the switching line:

$$S(t) = x(t) + \alpha \int x(t)dt = 0. \tag{28}$$

In Equation 28 above, α is equal to the eigenvalue of the closed loop feedback system. By differentiating Equation 28, we obtain

$$\dot{S}(t) = \dot{x}(t) + \alpha x(t) = 0. \tag{29}$$

For the feedback loop to have the sliding regime, we have to satisfy Lyapunov's stability condition, which is given by

$$S(t)\dot{S}(t) < 0. \tag{30}$$

This condition must be satisfied under all circumstances.

The Variable Structure Systems allow selection of control laws so that an unstable system can be stabilized by the controller. Another important property is that for the correct selection of the control function $u(t)$, the phase trajectory will converge to the switching line. When the representative point describing the initial state of the system (in this case the initial phase error, $\delta\Psi(t)$) reaches the straight line (Equation 28), then it will slide along the line until it hits the final steady state point (in this case the origin) on the phase plane. The behavior of the system will depend not on the system parameters but on the external parameter α shown in Equation 29 above. A suitable control law is

$$u(t) = -(k_1\,|x(t)| + k_0)\,\mathrm{sgn}\,S(t), \tag{31}$$

where $\mathrm{sgn}\,S(t)$ function is given by

$$\begin{aligned} S(t) &\geq 0 \qquad \mathrm{sgn}\,S(t) = 1 \\ S(t) &< 0 \qquad \mathrm{sgn}\,S(t) = -1 \end{aligned} \tag{32}$$

By substituting the system Equation 20 in Equation 29, and then using Equation 31 in place of $u(t)$, we get

$$\dot{S}(t) = -[k_1\,|x(t)| + k_0]\;\mathrm{sgn}\,S(t) + \alpha x(t), \tag{33}$$

where k_0 is a positive constant. Since the system parameter $b(t)$ is a positive quantity, to satisfy the Lyapunov stability condition dictated by Equation 30 above, we must select k_1 such that

$$k_1 > sup\left(\frac{\alpha}{|b(t)|}\right), \tag{34}$$

where "*sup*" is pronounced as "supremum." It means the constant k_1 must be higher than the greatest value of the ratio of the eigenvalue α, to the absolute value $b(t)$ of the system. Once the stability condition (Equation 30) is satisfied, the theory suggests that the sliding-mode exists and the feedback loop will be robust in relation to the change of parameters and load. The new feedback controller comprised by Equations 28 and 31 is shown in Figure 16. The expanded view of the controller structure is shown in Figure 17. As we can see from these figures, there are three constants in the controller which play an important role in the existence of the sliding mode conditions for reaching the sliding regime. We have investigated the controller properties, and the motion of the system in the phase plane is described in the following section.

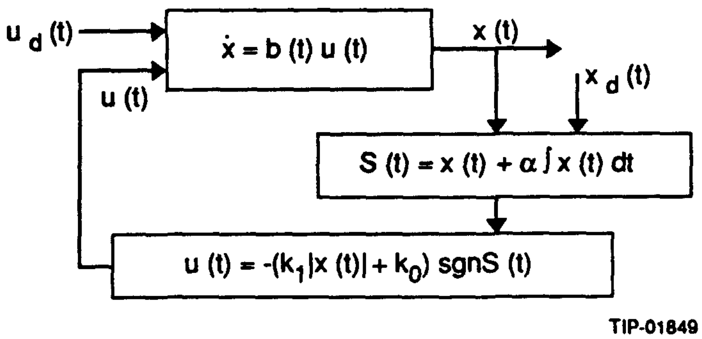

Figure 16. Block Diagram of the Feedback System for Digital Implementation.

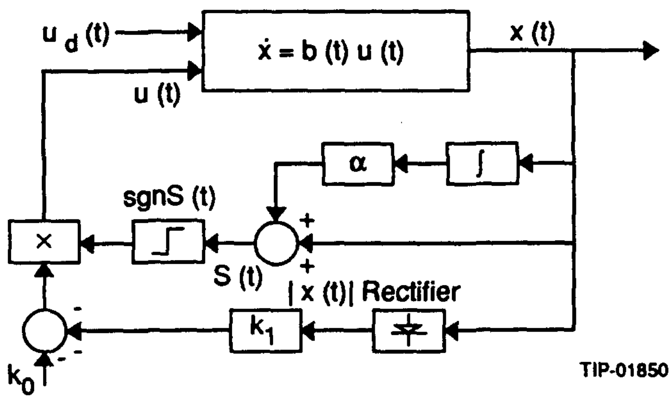

Figure 17. Block Diagram of the Feedback System for Analogue Implementation.

6.2 Analysis of the Loop Performance

At first the phase trajectories of Figure 15 are extended to include the control law described by Equation 31. The synthesis of the possible combination of closed loop system equations are shown in Table 1 below. The new phase trajectories are shown in Figure 18 for $k_0 = 10$ and $k_1 = 5$. The phase trajectories are not exactly straight lines due to the time variation in the system parameter $b(t)$. As we can see from this figure, the stable phase trajectories converge to a value bk_0 on the $\dot{x}$ axis. Also, the unstable phase trajectories start moving away from $(0, \pm bk_0)$ points. The significance of k_0 will be made clear later in the discussion. Table 1 shows all the modes of system equations we would encounter in the closed loop operation. If the constant k_1 is selected correctly, as dictated by Equation 34, then the stability of the closed loop system will be ensured. In the phase plane, a representative point set by the initial conditions will follow the family of the phase trajectories of the plane as in Figure 18 and would eventually converge to the origin. This point will be made clearer by using the simulated results shown in Figures 19 and 20.

Table 1. Closed Loop System Equations.

	$x(t) < 0$	$x(t) > 0$
$S(t) > 0$	$\dot{x} = bk_1x - bk_0$ III Quadrant	$x = -bk_1x - bk_0$ IV Quadrant
$S(t) < 0$	$x = -bk_1x + bk_0$ II Quadrant	$\dot{x} = bk_1x + bk_0$ I Quadrant

In the above figures we have plotted the variables x, $\dot{x}$ and S with respect to time for the first 8 ms with an initial phase error of 5 m. The curves shown in Figure 20 represent the phase trajectories; the arrows indicate the direction of motion of the representative point for the time response observed in Figure 19. The phase trajectories are shown up to 50 ms time period. The curves describing the motion of the system in the phase plane consist of two parts. The first part of the curve [point (a) in IV quadrant to point (b) in III quadrant in Figure 20] depends on the eigenvalue, α, feedback gain, k_1, and the initial conditions of the representative point. The salient points are also shown in Figure 19. From

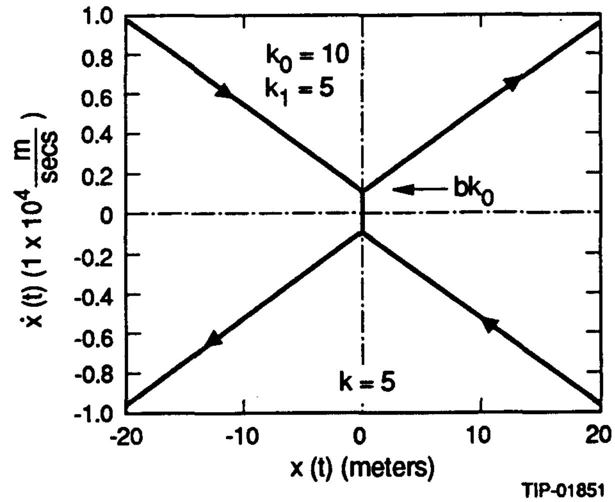

Figure 18. Phase Trajectories for Equations Shown in Table 1.

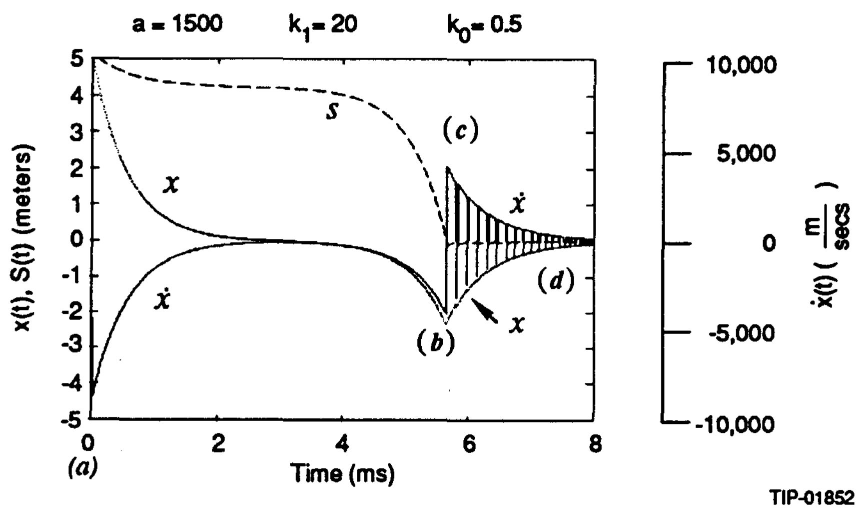

Figure 19. Variation of x, $\dot{x}$ and S for First 8 milliseconds.

point (a) to (b) in Figure 19 the sliding variable S is positive and time derivative is negative. Hence the Lyapunov's stability condition (Equation 30) is valid. When the sliding variable S becomes negative [at point (b)] the representative point has reached the switching line (Figure 20), the state of the system is now in the sliding regime. Here, since S is negative, $\dot{x}$ becomes positive, and the

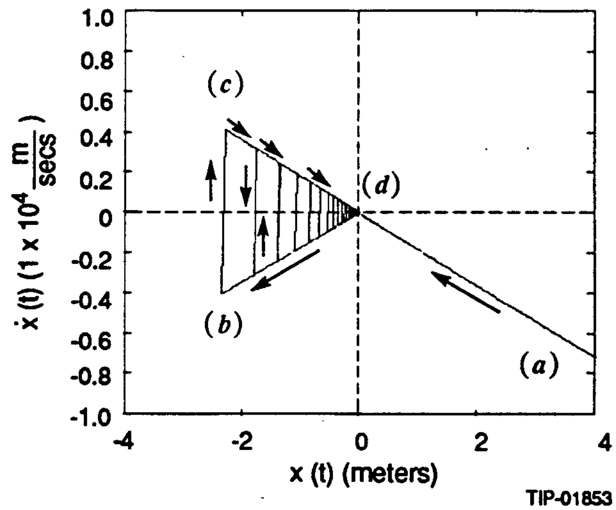

Figure 20. Phase Trajectories for the Time Response of the State Shown in Figure 19.

representative point has moved to point (c). From hereafter the motion is sliding on the switching line (Equation 28). We can see the sign of S changing more often. Everytime there is a sign change in S while sliding on the switching line, the trajectories jump from the II quadrant to the III quadrant. Even though the trajectories are pointing away from the origin in the III quadrant, the net effect is sliding. This is because the condition dictated by Equation 30 is the sufficient condition and is fully satisfied all along the sliding regime. The motion of the representative point will eventually converge at point (d). Thus the loop remains stable. Although $\dot{x}$ changes sign due to the control input u (the small frequency shift, δf), the output of the system, x, would not alternate in sign. In other words, there will not be chattering in the output variable. Also, the decay of the output from the point when the switching takes place [i.e., from point (b) to (d)] is controlled by the eigenvalue, α, which is independent of the system time constant.

In Figures 21 and 22 we have shown the plot of the decay of x and S with respect to time for α = 200 and 1500, k_1 = 3 and 20, and k_0 = 0.5 (fixed). In Figure 22, x is unstable for k_1 = 20, since it violated the condition shown by Equation 34. It is clear from these figures that the settling time is about $1/\alpha$. The frequency shift δf generated by the feedback controller and the expected variation on the radial orbit shift are shown in Figure 23. Since the frequency

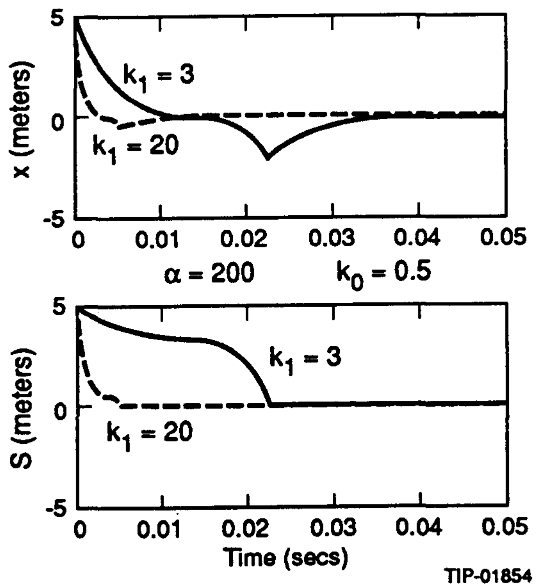

Figure 21. Decay of the State and the Sliding Variable, with $\alpha = 200$.

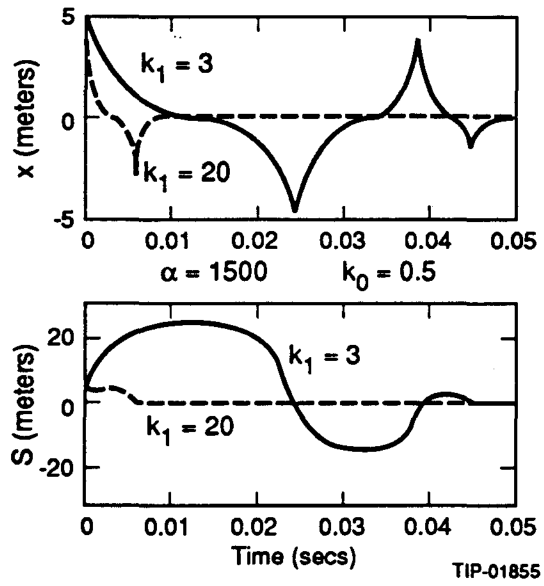

Figure 22. Decay of the State and the Sliding Variable, with $\alpha = 1500$. (Note the system is unstable for $k_1 = 3$.)

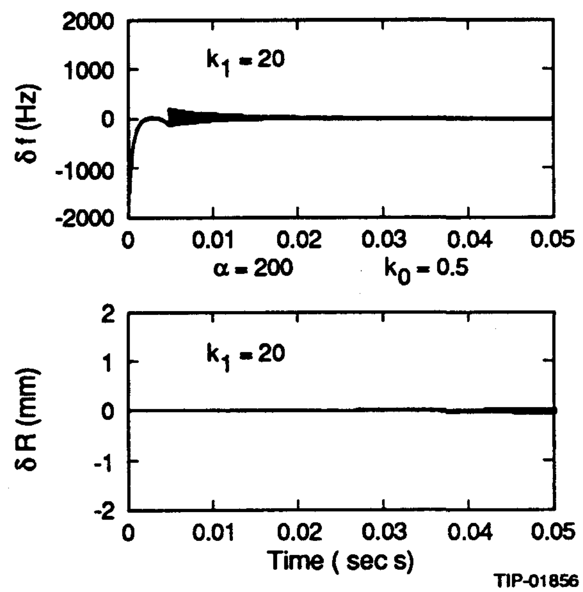

Figure 23. Decay of the Frequency Shift and the Radial Orbit Shift.

shift is alternating during the sliding regime, it may create unwanted beam excursions. However, the magnitude of these frequency oscillations can be controlled by adjusting the external feedback constants k_0, k_1, and α. We can see some advantages when k_1 is allowed to vary with time without breaching the stability condition. However, the best value of k_1 can be correctly selected by trial and error.

The robustness of the controller can be seen by subjecting the feedback system to an external disturbance u_d of 11 radians/sec. Time response of the state variable x with state feedback controller and sliding-mode controller is shown in Figure 24. The state variable x is held small (of course, alternating to a small amplitude) by the sliding mode controller; hence it shows the robustness against disturbance. It is also important to note that k_0 must be set slightly higher than u_d—the highest value of the expected disturbance (in this case, it was set at 11.8 in Figure 24). When there is disturbance, the feedback controller generates the control signal, u, such that it opposes the external disturbance signal. Since the constant k_0 controls the magnitude of disturbance rejection, it would be useful to have it set very high (say as high as 60, for 1 KHz disturbance rejection) as in Figure 25(a). The effect is not very encouraging since the time response of the state becomes more oscillatory near extraction. The oscillations cannot be damped by varying the constants [see Figure 25(b) and Figure 25(c)] unless we increase the sampling time as seen in Figure 25(d). Thus x has to be measured at four times the MEB revolution or more, which means fast electronics, in the case of digital implementation. Only higher sampling can cure this problem.

Figure 26 shows the time response of the state variable, x, for the system Equation 19, with the field error described by Equation 27, the disturbance signal of $u_d = 11$ radians/sec about 8 ms before extraction, and with 20% measurement error in the state x (i.e., $x_d = 0.2x$).

If we use the sliding-mode controller of the type described above in the feedback loop for an initial phase error of as much as 5 meters, Figure 23 shows a

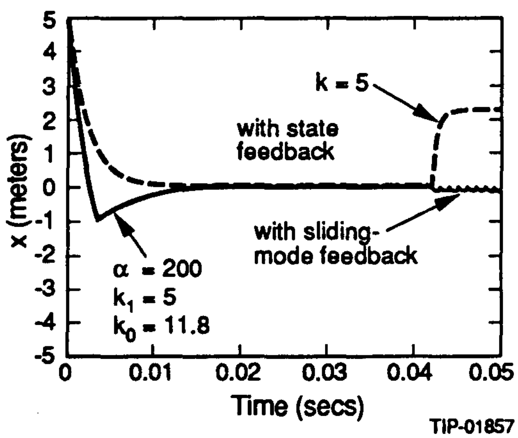

Figure 24. Time Response of the State with State Feedback and the Sliding Mode Feedback Under Disturbance, u_d.

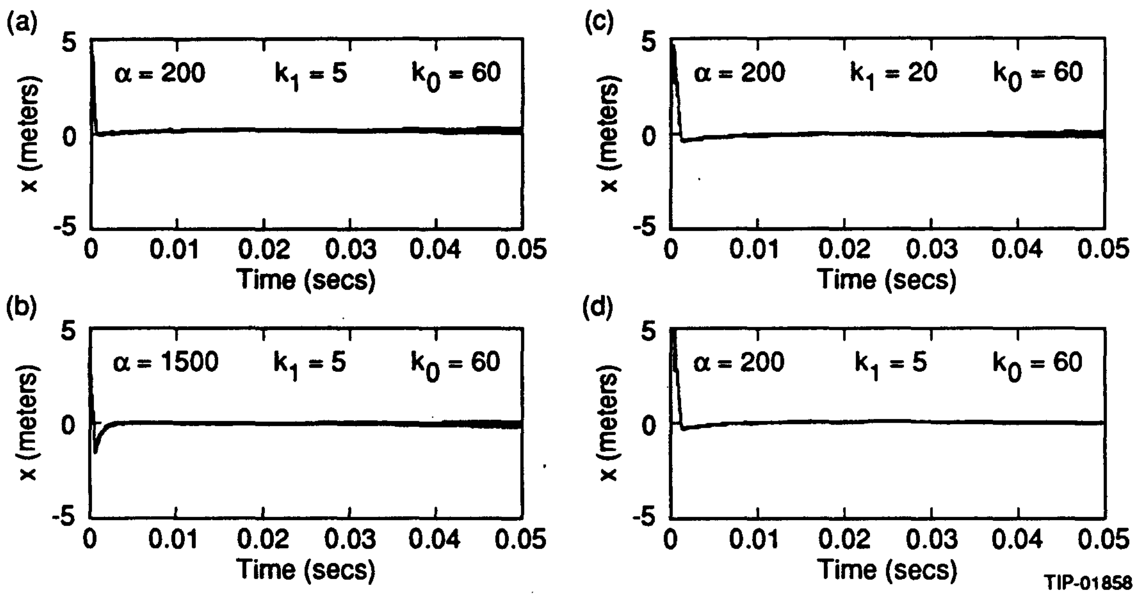

Figure 25. Time Response of the State to Reject Large Disturbance. (Measurement of the state is once every MEB revolution in (a), (b), and (c); in (d) the state is measured 4 times every MEB revolution.)

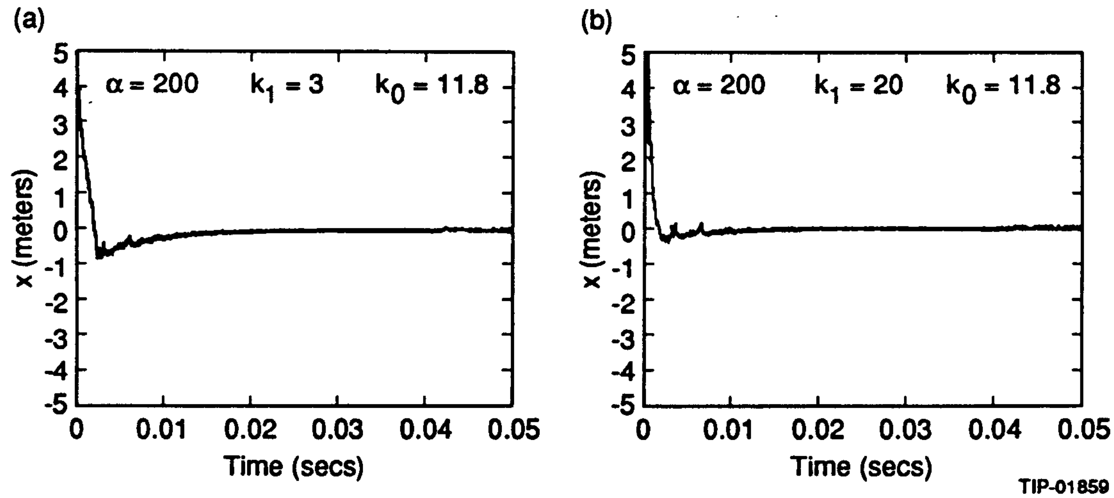

Figure 26. Time Response of the State with (a) and (b) Field Error (Equation 27) with Disturbance of $u_d = 11$ rad/sec as in Figures 13 and 24, and with 20% Measurement Error in the State x.

sudden frequency shift of 2KHz. This is predominantly set by the constant k_1. We can give a smooth change in the frequency shift by using time variation to k_1 such that it is initially small and then increases to a highest value. Also, the oscillations in the frequency shift after the sliding has taken place may be detrimental, since they may induce beam oscillations if the magnitude of the frequency shift is large. The alternative solution would be to design a more sophisticated sliding mode controller by dividing the control function u into two parts, a continuous part and a switching part. The continuous part holds the phase error to zero and behaves very much like the state feedback controller. Hence the frequency shift imposed by the feedback loop will not be oscillatory. The switching part introduces robustness into the loop and hence takes care of the disturbance rejection and problems related to measurement error. The oscillations in the frequency shift after the sliding has taken place will depend on the amount of disturbance rejection needed. Such a controller has been synthesized and will be reported elsewhere. However, it will be useful to study a simple model reference adaptive controller in the context of the single-input single-output feedback loop we have been discussing.

7.0 MODEL REFERENCE ADAPTIVE CONTROLLER

7.1 Selecting the Reference Model

A fundamental difference of the adaptive control with the state feedback controller is the way the stability of the overall system is defined for all initial conditions. A thorough analysis of the stable adaptive feedback systems is shown in Reference 10. This reference is thought to be more up-to-date at the time of writing this report. As we mentioned earlier, in this method of feedback control a reference model is needed. Since we know the parameter of the system to be controlled it will be easy to decide on the choice of the reference model. A suitable reference model for our feedback control problem can be described by the first order differential equation

$$\dot{x}_m = a_m x_m(t) + k_m r(t), \tag{35}$$

where the constant $a_m < 0$ and must be non-zero for reasons made clear later, k_m is another constant, and $r(t)$ is the reference signal which has to be non-zero and time-dependent, and is chosen such that the output of the reference model, $x_m(t)$, is close to the desired output from the system, $x(t)$. Now let us select the adaptive controller such that

$$u(t) = \theta(t)x(t) + k(t)r(t). \tag{36}$$

The block diagram consisting of the reference model and the adaptive controller is shown along with the system in Figure 27. The unknown parameters $\theta(t)$ and $k(t)$ are adjusted by the error signal obtained after subtracting the output of the reference model, $x_m(t)$, with the system output, $x(t)$, so that the loop automatically drives the error signal to zero. If we select $r(t)$, the reference signal, to be very small (say less than a centimeter peak) and time-varying, then the output of the system will be driven equal to x_m, since the error signal $e(t)$ is held zero by adjusting $\theta(t)$ and $k(t)$. The adjustment laws for $\theta(t)$ and $k(t)$

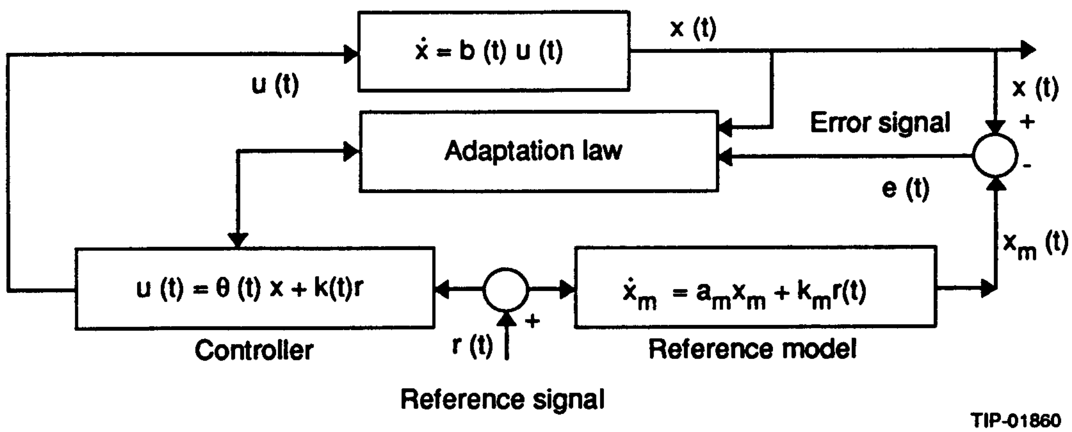

Figure 27. Block Diagram of the Model Reference Adaptive Controller.

are designed such that the goal of reducing the error signal to zero is met, and while doing so the entire system contains all signals within the limits. The design technique is shown below.

While designing $\theta(t)$ and $k(t)$, we assume that the system is time-invariant. Since the reference model output must generate the desired signal, the rule is to choose the controller parameters such that the combined transfer functions of the controller and the system are equal to the transfer function of the reference model for some values of $k(t) = k^*$ and $\theta(t) = \theta^*$. By substituting Equation 36 in the system Equation 20, the combined controller and system equation becomes

$$\dot{x}(t) = b\,\theta(t)x(t) + b\,k(t)r(t). \tag{37}$$

Comparing Equation 37 with the reference model Equation 35, we obtain

$$\theta(t) = \frac{a_m}{b} \equiv \theta^* \tag{38}$$

$$k(t) = \frac{k_m}{b} \equiv k^* \tag{39}$$

where θ^* and k^* represent the parameters of the adaptive controller at which the combined controller and system equation is equal to the reference model.

Equations 38 and 39 will be valid as long as $b > 0$; such is the case in our problem as shown in Figure 6. Since we need to determine adjustment laws for the adaptive controller parameters $\theta(t)$ and $k(t)$, let us define the error terms as follows:

$$e(t) = x(t) - x_m(t) \tag{40}$$

$$\xi(t) = \theta(t) - \theta^* \tag{41}$$

$$\vartheta(t) = k(t) - k^* \tag{42}$$

Since θ^* and k^* are some fixed values, their time derivatives are valid.

$$\dot{\xi}(t) = \dot{\theta}(t) \tag{43}$$

$$\dot{\vartheta}(t) = \dot{k}(t) \tag{44}$$

Let us represent $\dot{\theta}(t)$ and $\dot{k}(t)$ in terms of the error signal $e(t)$, state variable $x(t)$, and the reference signal $r(t)$, (since we know all these signals), and the system parameter b, and meanwhile satisfy the Lyapunov stability condition; then we would have completed the process of adjusting the controller parameters. Since we have three error equations, let the candidate for the Lyapunov function be

$$V(t) = \frac{1}{2}(e^2 + \xi^2 + \vartheta^2). \tag{45}$$

Differentiating the Lyapunov function with respect to time, we obtain

$$\dot{V}(t) = e\dot{e} + \xi\dot{\xi} + \vartheta\dot{\vartheta}. \tag{46}$$

For global stability of the loop and to achieve bounded signals for the controller parameters, Lyapunov stability theory requires the function $\dot{V} \leq 0$ (must be semi-definite) and the function $V > 0$ (must be positive-definite). To satisfy these conditions let us express the error signal $e(t)$ as follows:

$$\dot{e}(t) = \dot{x}(t) - \dot{x}_m. \tag{47}$$

Substituting Equations 35 and 37 in Equation 47 and making use of Equations 41 and 42, we obtain

$$\dot{e}(t) = b\xi(t)x + b\theta^* x - a_m x_m + b\vartheta(t)r(t) + bk^* r(t) - k_m r(t). \tag{48}$$

Using Equation 40 for $x(t)$ in Equation 48 and replacing a_m by $b\theta^*$ and k_m by bk^* from Equations 38 and 39, we obtain

$$\dot{e}(t) = a_m e + b\xi x + b\vartheta r. \tag{49}$$

Substituting Equation 49 in Equation 46,

$$\dot{V} = a_m e^2 + eb\xi x + eb\vartheta r + \xi\dot{\xi} + \vartheta\dot{\vartheta}. \tag{50}$$

By arranging

$$\dot{\xi} = -ebx = \dot{\theta}(t) \tag{51}$$

$$\dot{\vartheta} = -ebr = \dot{k}(t) \tag{52}$$

and setting $a_m < 0$, we can guarantee that $\dot{V} \leq 0$. Also, Equation 45 suggests that $V > 0$. Hence Equations 51 and 52 become the adaptive laws for the controller. After including the adaptive laws, the new block diagram is shown in Figure 28.

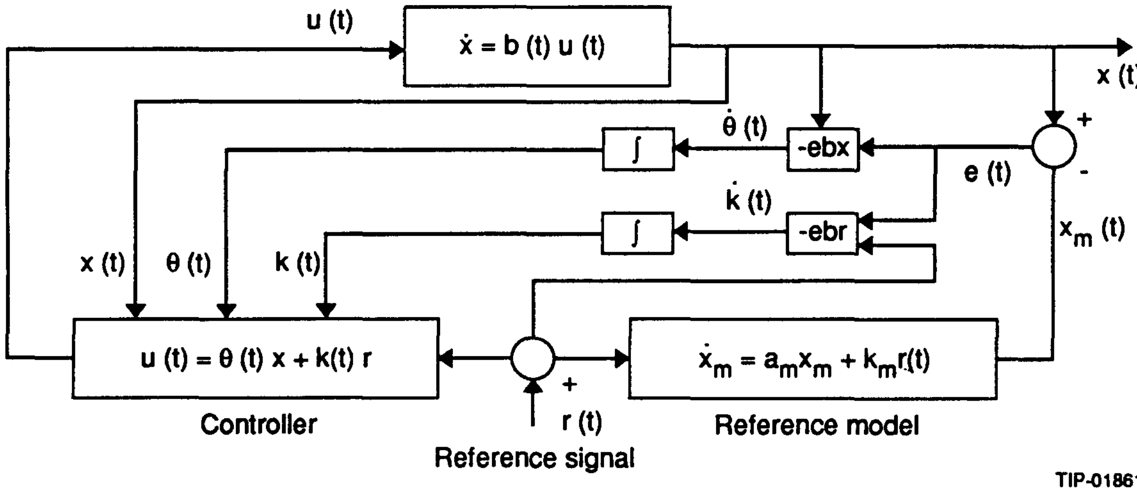

Figure 28. Model Reference Adaptive Controller.

7.2 Analysis of the Loop Performance

Simulations of the controller performance are carried out with the initial phase error of 5 meters and with $a_m = -200$, $k_m = 1$. The magnitude of the reference signal is chosen to be small and time-varying. The lowest frequency of the time-varying reference signal must be chosen at least about 10 times a_m. Figures 29 to 31 show different parameters of interest to the problem.

The adjustment law to the parameters of the controller [$\theta(t)$ and $k(t)$] depends on the state error signal $e(t)$, the state $x(t)$ and the internal reference signal $r(t)$. The parameter errors (Equations 41 and 42) do not necessarily converge to zero (see Figure 30), but may change more slowly with time.[10] The error signal $e(t)$ will converge to zero no matter what the controller parameter errors are. When the error signal is zero, we can say that the controller is adapting to system conditions. If we set the magnitude of the reference signal $r(t)$ small, then the reference model output will be small and hence the output of the system will be small. Convergence of the controller parameter errors to zero depends on the choice of the relevant reference signal. The interested reader is referred to Reference 10 for further discussion. In our simulation we have selected $r(t) =$

0.01 $[\sin(\omega t) + \sin(2\omega t)]$. The constant of the reference model, i.e., a_m, is selected close to the eigenvalue we used in our state feedback controller, which depends on the desired settling time of the state. Also, the constant k_m is selected based on the desired value of the steady state error.

In Figure 32 we have shown the time response of the state to the steady disturbance signal of amplitude $u_d = 11\,\text{rad/sec}$ imposed 8 ms before extraction. The feedback loop is trying to adapt to input disturbance but is taking longer, depending on the time constant of the reference model and the type of reference signal. By comparing Figure 32 with Figure 13, we see no such adaptation taking place with a state feedback controller. If we increase the gain of the adaptation process, then there would be sufficient reduction in the phase error. This is shown in Figures 33 and 34. These figures were plotted by multiplying Equations 51 and 52 by a constant k_a, which is set equal to 60. Since large adaptation gain increases the frequency shift (Figure 34), a suitable time variation to k_a may become necessary. However, the controller is not robust as compared to the sliding-mode feedback in Figure 24. The time response of the state with errors is shown in Figure 35 for the model reference adaptive controller. Recent advancements in achieving robustness for this type of controller are discussed in Reference 11. The major disadvantages with this controller are due to the stability problems associated with unmodelled dynamics. A computer simulation with the accelerator lattice code would be a good way to test the controller performance for all the known conditions. Since it will be a long time before we see this type of synchronization working, we are considering the proposal to simulate the performance using lattice codes.

8.0 PHASE MEASUREMENT

An accurate detection of the phase error is important to guarantee the controller operation. The phase error can be detected for one or two MEB turns depending on the magnitude of the error. Waiting for much longer than one MEB turn to measure the LEB phase could lead to large error. The consequence

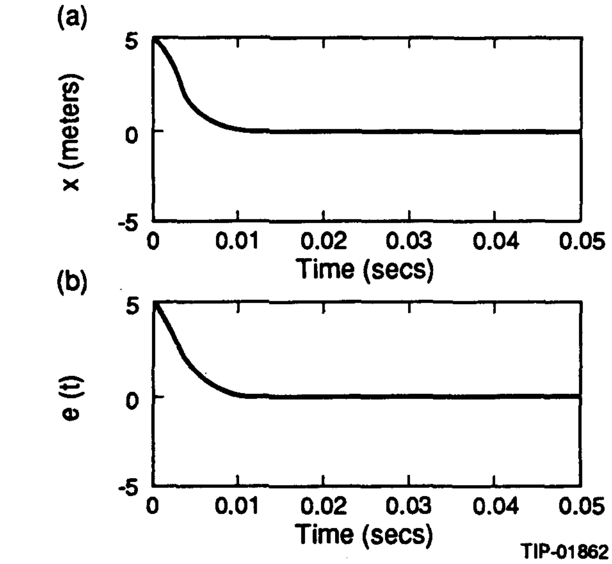

Figure 29. Decay of x (a) and e (b) with Respect to Time.

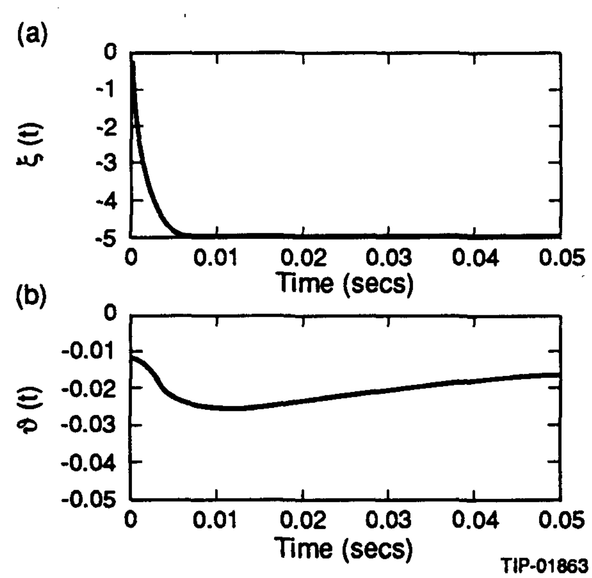

Figure 30. Decay of ξ (a) and ϑ (b) with Respect to Time.

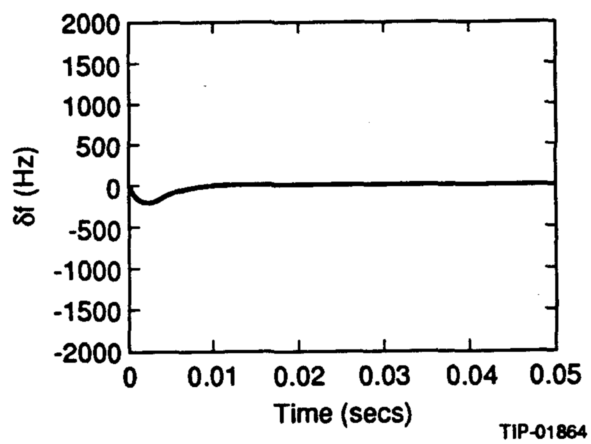

Figure 31. Decay of Frequency Shift with Respect to Time.

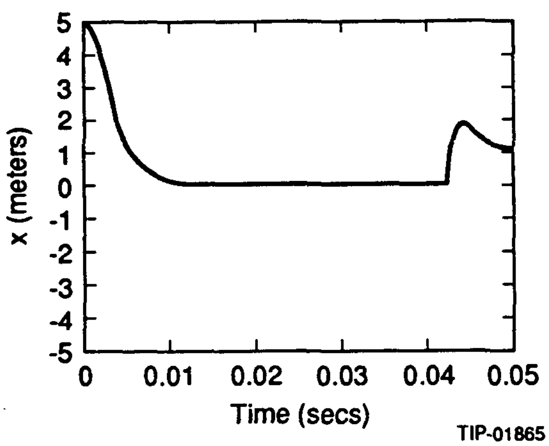

Figure 32. Time Response of the State Under Disturbance, u_d.

would be greater frequency shift generated by the feedback controller, which could lead to beam oscillations. The MEB completes about 3774 turns before it is ready to accept the beam from the LEB; if the phase is measured at every MEB turn, there will be 3774 points in the LEB cycle where the frequency shift

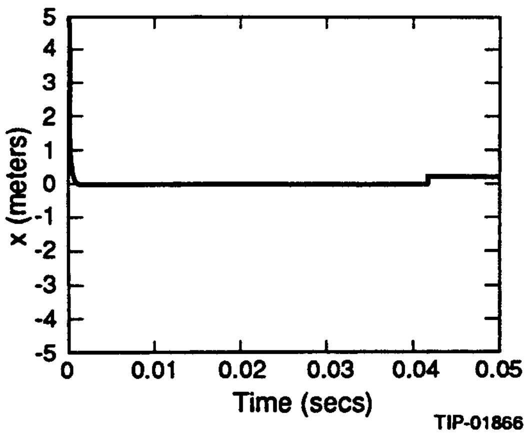

Figure 33. Time Response of the State Under Disturbance, u_d. (Adaptive gain, $k_a = 60$.)

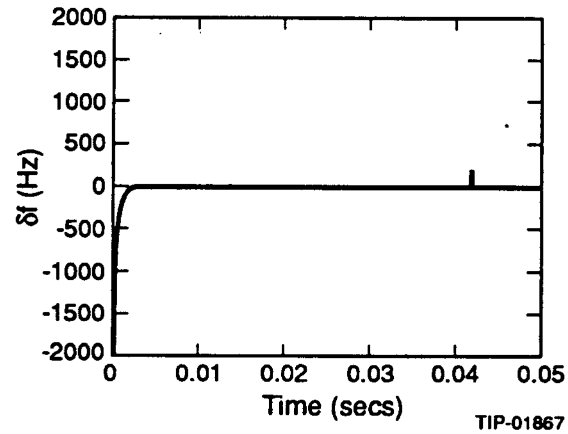

Figure 34. Decay of Frequency Shift with Respect to Time. (Adaptive gain, $k_a = 60$.)

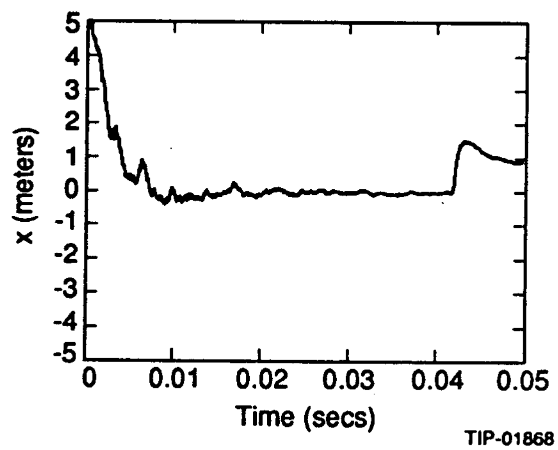

Figure 35. Time Response of the State with Field Error (Equation 27) with Disturbance of $u_d = 11\,\text{rad/sec}$ and 20% Measurement Error in the State x.

has to take place. This is possible if the hardware can extract the phase error from the measured LEB phase and then solve the controller algorithm within the available time. One of the ways the LEB phase can be measured approximately is by time-tagging the arrival time of the LEB reference wave from the instant the MEB reference wave completes the turn. In the development system considered here, a Time-to-Digital Converter (TDC) will be used to record the arrival time of the LEB reference wave. Using this time of flight information, the phase of the LEB reference wave is calculated in terms of the path length by using the following equation:

$$\Psi'_{\text{measured}}(t) = 2\pi[R + \delta R(t)]\,\frac{f(t) + \delta f(t)}{h}\,\tau' \tag{53}$$

where τ' is the arrival time of the LEB reference wave, $\delta f(t)$ is the frequency shift of the LEB frequency in the previous MEB turn, and $\delta R(t)$ is the average radial position offset during the time-tagging period. Equation 53 assumes no frequency shift while measuring the arrival time of the LEB reference wave. The phase error is calculated by subtracting the measured LEB phase values from those shown in the "trip-plan" earlier for a given MEB turn. We are considering the possibility of using a Digital Signal Processor to extract the phase error and compute the frequency shift. We have done the computer simulation of the above concept using two rf waves. The rf wave representing the MEB rf signal was running at the MEB injection frequency, and the other rf wave frequency was varied between 47.518 MHz and 59.776 MHz in 50 ms. We stepped through the time signals at 1 nanosecond time interval with the initial LEB rf wave offset in phase equivalent to 5 meters in space. We extracted the phase information using Equation 53. The results of simulations are encouraging.

9.0 CONCLUSIONS

A scheme is outlined for locking the phase of a selected rf wave in the Low Energy Booster to a selected rf wave in the Medium Energy Booster. A mathematical model is derived to design the global feedback controller which is expected to adjust the relative phase of the selected rf waves in two rings and also to maintain low radial orbit shift. The control parameters are (1) the rf signal frequency and (2) the phase of the beam bunch with respect to the zero crossover of the rf wave. The presence of field errors (both electric and magnetic) can be considered as disturbance to the controller.

The controller design problem becomes more complex when all the feedback loops affecting the synchronization are considered. To understand the problem clearly, we considered only the control of the synchronizing phase by varying the accelerating frequency and leaving the radial feedback loop open. In a final scheme, however, we need to include the radial steering loop. A linear state feedback controller is compared with the modern sliding-mode and model reference adaptive controllers. From the disturbance rejection point of view due to field errors, it can be concluded that the sliding-mode controller is good, but it *may* introduce beam oscillations unless we modify the algorithm shown in this report. Although the model reference adaptive controller is undergoing adaptation, it does not guarantee local stability when we introduce the second feedback loop.[10] Also, the model reference controller lacks ability to generate a good control signal when the system is not accurately modelled. Furthermore, to alleviate the switching effects in the sliding-mode controller, we have identified a scheme which would combine the sliding-mode properties with the linear state feedback controller. This is done by superimposing the switching part on the state feedback controller to achieve the robustness due to field errors.

ACKNOWLEDGEMENT

Discussions with K. S. Yeung are gratefully acknowledged.

REFERENCES

1. J.A. Dinkel et al., "Synchronous Transfer of Beam from the NAL Fast Cycling Booster Synchrotron to the NAL Main Ring System," *IEEE Transactions on Nuclear Science*, **NS-20**, 3, (June 1973).
2. Y. Kimura et al., "Synchronous Transfer of Beam from the Booster to the Main Ring in the KEK Proton Synchrotron," *IEEE Transactions on Nuclear Science*, **NS-24**, 3, (June 1977).
3. Site-Specific Conceptual Design, SSCL-SR-1056, July 1990.
4. B.C. Kuo, *Automatic Control Systems*, Prentice-Hall, 1981.
5. Thomas Kailath, *Linear Systems*, Prentice-Hall, 1980.
6. U. Itkis, *Control Systems of Variable Structure*, John Wiley & Sons, New York, 1976.
7. V.I. Utkin, "Variable Structure Systems with Sliding Modes," *IEEE Transactions on Automatic Control*, **AC-22**, 2, (April 1977).
8. K.S. Yeung et al., "A New Controller Design for Manipulators Using the Theory of Variable Structure Systems," *IEEE Transactions on Automatic Control*, **33**, 2, (February 1988).
9. B. White, Lecture Notes on Variable Structure Systems, Dept. of Electrical Engineering, University of Bath, Bath, U.K., 1985.
10. K.S. Narendra et al., *Stable Adaptive Systems*, Prentice-Hall, 1989.
11. C.M. Ha et al., "Full-State Model Reference Adaptive Control in the Presence of Bounded Disturbance and Noise," J. Guidance and Control, submitted for publication (1990).